Exp. Theo. NANOTECHNOLOGY 10 (2026) 289-300 https://doi.org/10.56053/10.S.289

Sol–gel-derived mullite nanoparticles: Structural and antibacterial insights

Ameen Khaleefah[1], *Mohammed RASHEED*[2,*]

[1]Applied Sciences Department, University of Technology- Iraq, Baghdad, Iraq
[2] College of Production Engineering & Metallurgy, University of Technology- Iraq, Baghdad, Iraq.
[*]) Email: rasheed.mohammed40@yahoo.com

Received 17/11/2025, *Received in revised form* 15/12/2025, *Accepted* 28/12/2025, *Published* 15/2/2026

Mullite ($3Al_2O_3 \cdot 2SiO_2$) is synthesized via a controlled calcination process at 950 °C and comprehensively characterized using multiple advanced techniques to establish its structural and functional properties. AFM analysis revealed densely packed grains with irregular morphology, significant surface roughness (Z-axis variation ≈ 767 nm), and an average grain size of ~85 nm, while FESEM confirmed the presence of nanoscale particles uniformly distributed alongside larger agglomerates, yielding a moderately broad size distribution (17–167 nm, average ~100 nm). TEM micrographs provided direct evidence of discrete nano crystallites with a narrow size distribution (17–49 nm, average ~30 nm), highlighting the distinction between primary crystallites and surface grains. The complementary nature of AFM, FESEM, and TEM results demonstrated the multi-scale particle organization in mullite, ranging from nano crystallites to secondary aggregates. Antibacterial activity is systematically evaluated against *Escherichia coli* and *Staphylococcus aureus* using both agar diffusion method (ADM) and spread plate method (SPM). The results revealed complete inhibition of bacterial growth (0 colonies) in SPM and the absence of inhibition zones in ADM, indicating the strong antibacterial efficacy of 950 °C-fabricated mullite pellets. These findings emphasize the potential of mullite as a multifunctional material, combining nanoscale structural control with promising antimicrobial activity for biomedical and environmental applications.

Keywords: Sol–gel technique; SEM; AFM; *E.coli*.

1. INTRODUCTION

Many fields including materials science, healthcare and environmental protection have greatly benefited from the emergence of nanotechnology. Aluminum oxide (Al_2O_3) and silicon dioxide (SiO_2) are prominent in a wide range of nanomaterial properties that can be exploited in catalytic applications, ceramic-based applications, electronics, medicine, etc [1-3]. Their unique properties of thermal stability, chemical inertness, tensile strength and biocompatibility make them indispensable for modern technology and medical applications [4,5]. Mullite, a composite material of Al_2O_3 and SiO_3, is widely used structurally and functionally, and is mostly considered for its high temperature resistance and extremely low thermal expansion [6]. The use of sol-gel process for the synthesis of nanomaterials provides a simple and flexible route for materials with high control over composition, size and shape [7]. This is a hydrolytic condensation hydrolysis reaction, converting alkoxides or metal salts into a gel-like state that becomes nanostructured materials upon heating [8]. Homogeneous particle dispersion: Homogeneous materials can be synthesized by sol-gel technology at relatively low temperatures, and this work has produced nanoparticles of Al_2O_2, SiO_3 and mullite by sol-gel method Tetraethyl orthosilicate (TEOS, $Al(NO_2)_2$•$9H_2O$ and citric acid are used as starting materials) [9,10]. Nanotechnology is applied in the design of novel antimicrobials, which is particularly important in light of the increasing resistance of bacteria to antibiotics [11]. Studies have shown that nanoparticles induce reactive oxygen species, and in interaction with bacterial membranes inhibit the proliferation or activity of pathogens [12]. Antibacterial therapies are urgently needed, given the unique physicochemical properties of novel nanomaterials that should be exploited through nanotechnology [13]. The relevant properties of aluminum oxide and silicon dioxide nanoparticles as well as mullite ($3Al_2O_3.2SiO_2$) are combined with respect to their suitable antibacterial performance and their established applications due to their stability, biocompatibility and reactivity [14]. This requires synthesis strategies that allow uniform access to highly pure nanoparticles, with well-defined shapes to be performed in this design domain [15]. The sol–gel method is a highly efficient and versatile technique for synthesizing nanoparticles with precise control over size, composition, and homogeneity at the nanoscale. Despite its proven success in producing various nanomaterials, its application for synthesizing antibacterial Al_2O_3, SiO_2, and mullite ($3Al_2O_3 \cdot 2SiO_2$) nanoparticles remains relatively limited [16]. Although Al_2O_3 and SiO_2 nanoparticles have demonstrated strong antibacterial potential, especially due to their surface reactivity and ability to generate reactive oxygen species (ROS), the sol–gel route has not been widely adopted in their antibacterial-focused fabrication. Most reported studies have employed physical or chemical vapor-based methods instead. Therefore, exploring the sol–gel method for preparing Al_2O_3, SiO_2, and mullite nanoparticles offers a promising pathway to achieve cost-effective, uniform, and high-purity nanomaterials with potential applications in antibacterial coatings, biomedical devices, and environmental protection systems [6]. An important gap in our knowledge is the relationships between nanoparticle morphology and antibacterial activity. Bridging these gaps would be an important step towards the development of nanotechnology-based means to combat bacterial infections [17]. Many types of nanoparticles have been successfully synthesized by sol-gel technology which allows precise control of composition, size, morphology etc. The method is based on starting materials (metal alkoxides or salts) and allows the formation of nanostructured materials in a highly pure and homogenous dispersion. Furthermore, as the resistance of bacteria to antibiotics has been growing, it has triggered a new path in the development of antimicrobial agents and nanoparticles have become a new choice in order to interfere with the bacteria growth [18].

The current work is concerned with the production of the nanoparticles of Al2O3, SiO4, and mullite ($3Al_2O_32SiO_4$) using the sol-gel technique and the exploration of their structural characteristics and antibacterial activity [19]. A major aspect in the discovery of new therapeutics is the production of nanomaterials that can target antibiotic-resistant pathogens including *Escherichia coli* and

Staphylococcus aureus. This study employs the rapid/precise procedures to create oxide nanoparticles with the aim of assisting to accumulate information about the antibacterial activity as the antibacterial potential of oxide nanoparticles [20]. Synthesis and characterization of nanoparticles are a pivotal focus because the sol-gel method has only very high homogeneity and shape-controlled materials in the deposits, to grow nanoparticles with well-defined structure, high-quality precursors like TEOS, Al(NO39H2O) and anhydrous citric acid are used [21]. The behavior of nanoparticles as antibacterials designed by the use of Al2O3, SiO4 and mullite in-depth studies will be assessed in this study will focus on their impact on E. coli and Staphylococcus aureus growth inhibition [22]. Experimental experiments will be conducted to verify the efficacy of the antibacterial properties in the diameters of the inhibition zones and the efficiency ratio under various concentrations [23, 24]. In this study, there is also the effort to compare the antibacterial properties of the materials of Al2O3, SiO4 and mullite nanoparticles in order that you choose which one of these materials is more viable to use in the future. The purpose of the study is to demonstrate the distinctive characteristics and mechanisms of individual nanoparticles to enable optimum application in the application of antibacterial use. The outcomes of this work should be able to propose new modalities to fight against the multidrug-resistant microorganisms hence develop the sphere of nanomedicine.

2. EXPERIMENTAL

2.1 Materials

The experiment is conducted on various chemicals which included, double-distilled water, anhydrous citric acid (CA, $C_6H_8O_7$) Sigma-Aldrich, ethanol (C_2H_6O), tetraethoxysilane of Sigma-Aldrich, 99.95% pure; Aluminum Nitrate Nonahydrate 98.99%. The chemicals are fully purified Sigma- Aldrich purity as purchased without further purification. Their primary focus is to obtain high-purity chemicals as they will guarantee that nanoparticles synthesis will be free of any interference and will promote their structural and functional characteristics. In the case of sol-gel, it is observed that citric acid complexes with silicon oxide precursor-Teledor [TEOS] and aluminum nitrate. The reaction process necessitates this complexation, resulting in precursor homogeneous dispersal and therefore the ultimate nanoparticles quality. The conditions of preparation and ratios of reagents used in the synthesis, especially the molar ratio is of special concern to achieve nanoparticles with specific characteristics. The objective of the study is to control these parameters in order to attain the effective nucleation of the nanoparticles and possibly to justify their characteristics to use it in future.

2.2 Synthesis of Al_2O_3 and SiO_2

The synthesis of mullite ($3Al_2O_3•2SiO_2$) is accomplished using the sol-gel method. Initially, 100 mL of distilled water is utilized to dissolve equivalent amounts of tetraethoxysilane (TEOS, $C_8H_{20}O_4Si$) and aluminum nitrate nonahydrate ($Al(NO_3)_3•9H_2O$). Citric acid is then added to the solution to chelate the metal ions, maintaining a 1:1 molar ratio, which ensured uniform distribution of the metals and facilitated effective removal of residual water. During 80°C heating, a magnetic stirrer swirled the mixture. This made it thick gel. After drying and heating to 200 °C, the gel became powder. This powder is calcined to 950 °C in a muffle furnace. Heat continued until the powder became white, indicating crystal formation. This high temperature created mullite and stabilised nanoparticles. This prevented shape change and maintained them operating properly.

2.3 Characterization

A scanning electron microscope (SEM) examined nanoparticle form. A carbon grid is coated with a tiny coating of gold before testing to boost sample conductivity. The SEM pictures exhibited nanoparticle surface, shape, and size. A Beckman Coulter SA-3100 BET analyzer is used to determine the surface area of CM and SM mullite samples by measuring nitrogen adsorption. Nanoparticle size

and surface topography are analyzed using a Shimadzu atomic force microscope (AFM) operating in tapping mode. The high-resolution 3D photos validated the particles' tiny size and atomic-scale features. The AFM scans demonstrated that nanoparticle surfaces are uniform, supporting the SEM investigation. Transmission electronic microscopy (TEM) type Zesis-EM10C-100 KV, made in Germany.

2.3.1 Antibacterial activity

Using an original method, we performed the following tests on whether Aluminum oxide nanoparticles (Al_2O_3-NPs) wanted to break down microorganisms. Hence; Gram-negative *Escherichia coli* (*E. coli*) and Gram-positive *Staphylococcus aureus* (*S. aureus*) are examined to see if the nanoparticles could be lethal to them. To ensure reproducibility of results, bacterial suspensions are standardized to the 0.5 McFarland turbidity standard prior to testing. A 10% (w/v) solution of aluminum oxide (Al_2O_3) nanoparticles is prepared by dissolving 1 g of the nanopowder in 10 mL of dimethylformamide (DMF). Sterile 5 mm diameter filter paper discs are then impregnated with the Al_2O_3 nanoparticle solution under aseptic conditions. Following preparation, the discs are carefully placed onto Mueller–Hinton agar plates that had been previously seeded with the standardized bacterial isolates. The plates are incubated at 37 °C for 24 hours. After incubation, the diameter of the inhibition zones surrounding each disc is measured in millimeters to assess the antibacterial efficacy of the Al_2O_3 nanoparticles. The results revealed that Al_2O_3 nanoparticles effectively inhibited the growth of pathogenic bacteria, indicating their promising potential as a broad-spectrum antibacterial agent.

3. RESULTS AND DISCUSSION

3.1 Field emission scanning electron microscope (FESEM)

FESEM micrograph of mullite calcined at 950 °C (Fig. 1a) reveals a heterogeneous surface microstructure consisting predominantly of fine nanoparticles dispersed across the substrate, interspersed with larger agglomerates and block-like crystallites. The nanoscale particles appear nearly spherical in shape, indicating effective nucleation during calcination, while the presence of larger aggregates suggests localized grain growth and partial sintering. Such features are typical of mullite synthesized at intermediate calcination temperatures, where both primary crystallites and secondary agglomerates coexist. The uniform distribution of smaller particles across the matrix reflects a controlled thermal process, while the irregular clusters highlight the onset of surface coarsening and densification.

Quantitative particle size analysis based on 250 measurements (Fig. 1b) shows that the mullite particles span a range from ~17 nm to 167 nm, with an average size of ~100 nm and a standard deviation of ±25.3 nm. The histogram presents a moderately broad, near-Gaussian distribution, with the majority of particles concentrated between 80–120 nm. Compared with TEM results (average ~30 nm) and AFM analysis (average ~85 nm), the FESEM data emphasize the detection of larger secondary grains and aggregates rather than isolated crystallites. This is consistent with the sensitivity of FESEM toward surface texture and agglomerated features, providing complementary insight into the multi-scale particle organization of mullite [25, 26].

The combination of fine nanoscale crystallites and larger aggregates is advantageous for multifunctional performance. The smaller particles enhance surface reactivity and active sites, which are beneficial for catalytic and antibacterial applications, while the larger grains contribute to structural stability and mechanical robustness. The particle size distribution at 950 °C therefore reflects an optimal balance between high surface area and microstructural integrity, aligning with the desired characteristics of mullite for advanced engineering and biomedical uses.

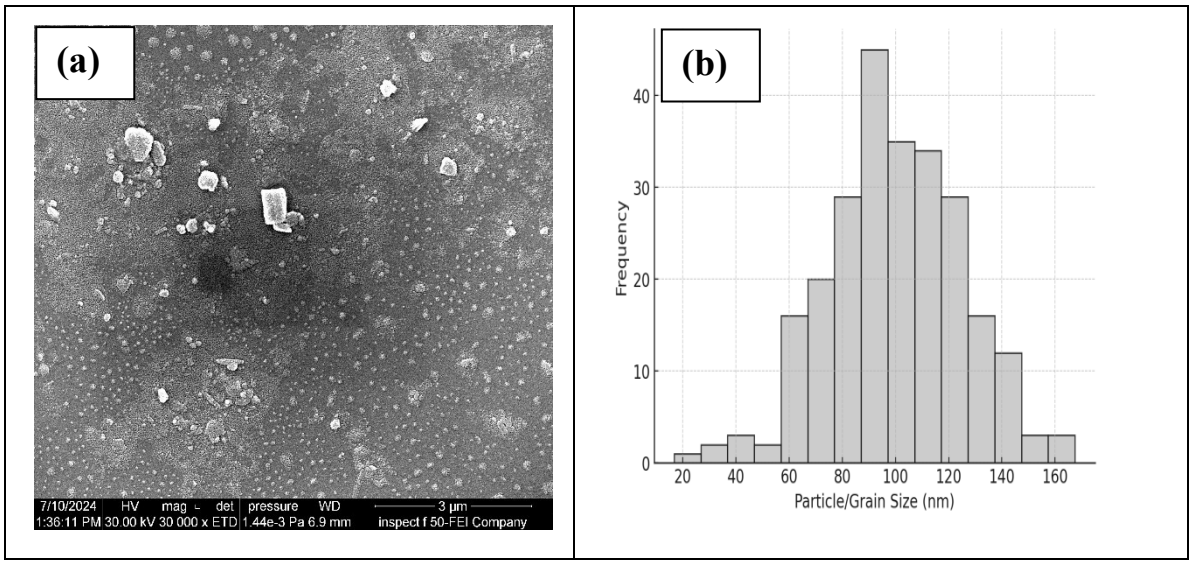

Figure 1 (a) SEM mullite image, and (b) Distribution particles of 950 °C-fabricated.

3.2 Atomic force microscope (AFM)

The AFM micrograph (2D and 3D) of mullite calcined at 950 °C (scan area: 7.54 × 7.54 µm²) shows a surface composed of densely packed grains with irregular and non-uniform morphologies. The grains exhibit pronounced height variations, producing a roughened surface texture consistent with thermally induced grain growth and partial coalescence at high calcination temperatures. The mullite pellet calcined at 950 °C exhibited a surface roughness average (Sa) of 170.32 nm and a root mean square roughness (Sq) of 210.51 nm, indicating a moderately coarse surface topography characteristic of thermally treated ceramic materials. The Z-axis roughness (≈767 nm) confirms the presence of significant vertical topography, highlighting the heterogeneity of the surface (Fig. 2a and b). Statistical analysis of 250 grains extracted from the AFM image shows particle sizes ranging between ~20 nm and 137 nm, with an average grain size of ~85 nm and a standard deviation of ±20.3 nm. The histogram (Fig. 2c) reveals a broad, near-Gaussian distribution with most of the grains are predominantly distributed within the size range of 70–100 nm.

The broader size distribution can be attributed to AFM's sensitivity to particle agglomerates and surface grain boundary features, which tend to highlight surface coarsening effects rather than the dimensions of individual crystallites. The data suggest that mullite pellets at 950 °C undergo grain enlargement, leading to surface features with higher variability. The AFM results emphasize the role of calcination temperature in determining surface roughness and grain size evolution. Larger grains and higher roughness are expected to influence functional properties such as surface energy, wettability, and bacterial adhesion, thereby complementing the antibacterial outcomes observed in spread plate tests [27,28].

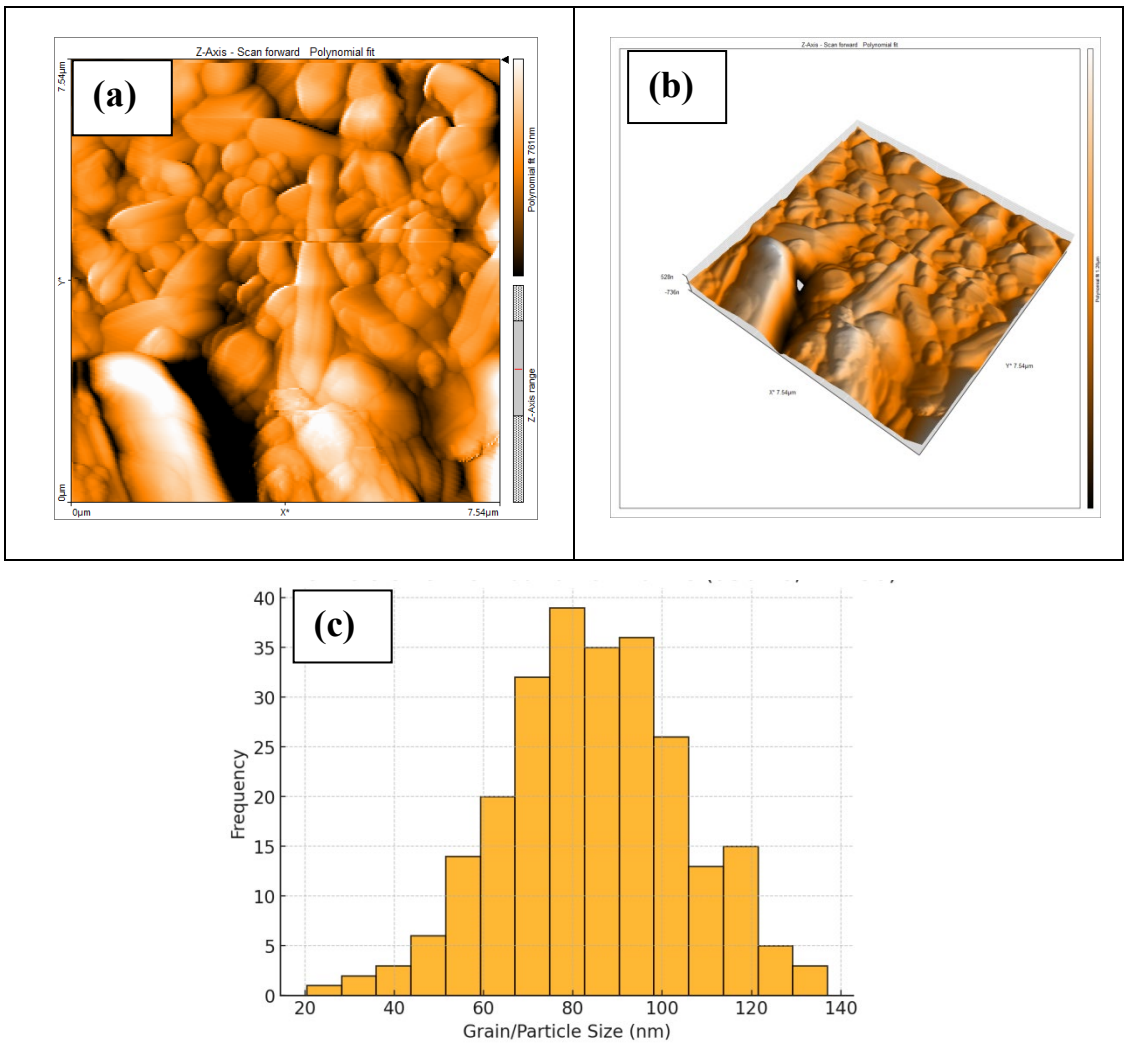

Figure 2 (a) Two-dimensional (2D) AFM topographic image, (b) three-dimensional (3D) AFM surface morphology, and (c) particle/grain size distribution histogram of mullite pellet calcined at 950 °C

3.3 TEM analysis

The TEM micrograph of mullite calcined at 950 °C reveals nanosized grains with a tendency toward irregular morphology and partial agglomeration. The particles are generally well separated, with moderate clustering indicative of thermally driven sintering effects. The contrast variation confirms crystallinity, and the nanoscale size range demonstrates that mullite formation occurs effectively at this calcination temperature. To quantify particle size, a statistical analysis is performed using 250 particles. The histogram (Fig. 3 a and b) show that particle diameters are distributed between ~17 nm and 49 nm, with an average size of ~30 nm and a standard deviation of ±4.8 nm. The distribution follows a near-normal profile, with the majority of particles clustered in the 25–35 nm range. This indicates that mullite nanoparticles at 950 °C maintain a relatively narrow size distribution, reflecting good control of nucleation and growth during calcination. The absence of extremely coarse particles suggests that grain coalescence remains limited, preserving nanoscale dimensions suitable for surface-dependent applications. The nanoscale size (~30 nm) coupled with the uniform distribution is particularly important for functional properties such as surface reactivity, antibacterial activity, and dielectric performance. Smaller particles with high surface-to-volume ratios enhance interfacial interactions, making mullite synthesized at this temperature promising for advanced engineering and biomedical applications. This broader size distribution compared to TEM results (~30 nm average) can

be attributed to AFM's sensitivity to agglomerates and grain boundary features, which reflect surface coarsening effects rather than individual crystallites [29,30].

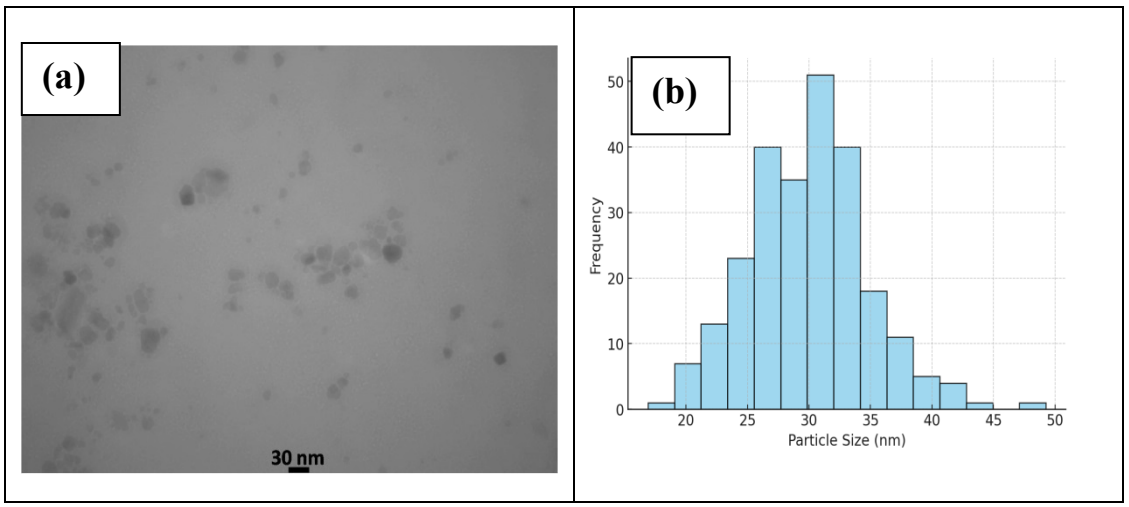

Figure 3 TEM micrographs of mullite nanoparticles calcined at 950 °C: (a) Low-magnification image showing the general morphology and dispersion of the nanoparticles and (b) Particle size distribution histogram.

3.4 Mechanism of antibacterial activity

As demonstrated in Figure 4, α-Al_2O_3 and SiO_2 nanoparticles are bactericidal due to their cationic size and reactive oxygen species (ROS) production. Due to their ionic and structural features, nanoparticles interact with bacterial cell membranes. Their positively charged groups strongly electrostatically interact with negatively charged bacterial membranes, penetrating and disintegrating cell walls. The contact destroys the bacterial membrane, inactivating the cell. Nanoparticles may create ROS, which damage bacterial proteins, lipids, and DNA. Another technique is lipopolysaccharide-containing bacterial outer membrane nanoparticle "self-promoted uptake". Cytoplasmic membrane channels may slow bacterial metabolism and kill cells. These techniques demonstrate α-Al_2O_3 and SiO_2 nanoparticles' antibacterial properties [31-34].

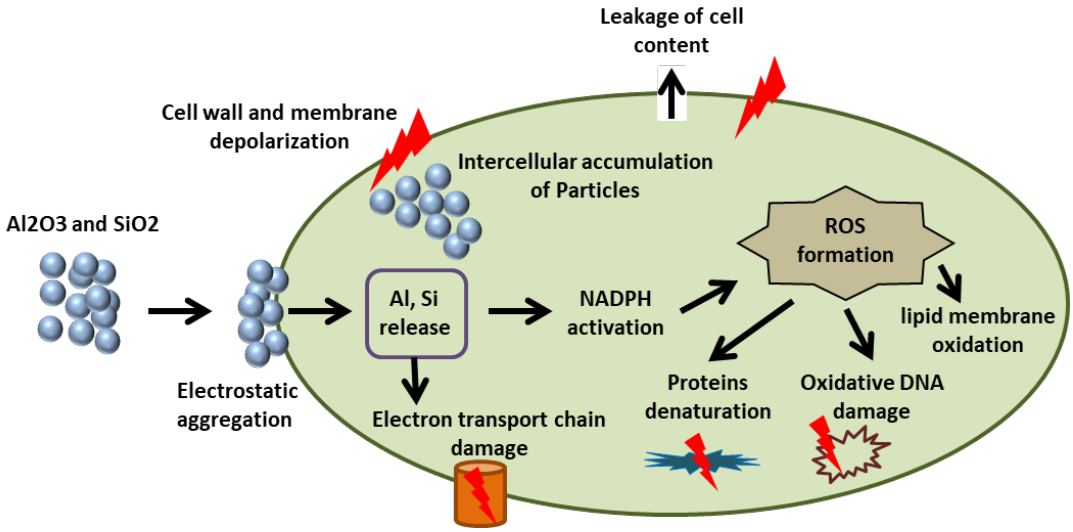

Figure 4 950 °C-fabricated mullite sample antibacterial mechanism.

3.5 Antibacterial activity

Figure 5 illustrates the Agar well diffusion tested 950°C-produced mullite pellets for antibacterial activity against *Escherichia coli* and *Staphylococcus aureus*. Using 0.3 g pellets, *E. coli* and *S. aureus* inhibition zones are 12 and 13 mm. Mullite pellets killed Gram-negative and Gram-positive bacteria, although E. coli is more aggressive. *E. coli's* weaker peptidoglycan layer permits nanoparticles through its cell wall more than Gram-positive bacteria like *S. aureus* Mullite pellets may inhibit bacteria via ROS generation and electrostatic interactions between positively charged nanoparticles and negatively charged bacterial membranes [31].

Agar well diffusion method (ADM), Pellet-Mullite at 1100 ºC				
No.	**Bacteria Type**	**Weight (g)**	**Zoom (mm)**	**Image**
1	*E-coli*	0.3	12	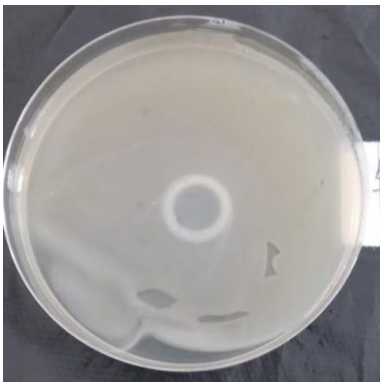
2	*S. aureus*	0.3	13	

Figure 5 Agar well diffusion is used to evaluate *E. coli* and *S. aureus* in 950 °C mullite pellets.

3.5.1 Spread plate method (SPM)

Figure 6 presents results from an experiment using the spread plate method (SPM) to analyze the growth of two types of bacteria, *Escherichia coli (E. coli*) and *Staphylococcus aureus* (*S. aureus*), on a powder-mullite substrate at a temperature of 950 °C. Each bacterial type is tested with 0.3 grams of the sample. The results show that for both *E. coli* and *S. aureus*, 0 colonies are observed, indicating complete inhibition of bacterial growth on the substrate [30-35]. These results prove the assumption that the powder-mullite substrate at 950 ºC has a strong antibacterial property with Gram-negative (*E. coli*) and Gram-positive (*S. aureus*) bacteria [36-40]. The non-formation of colonies indicates that under these calcification conditions, mullite physically-chemically properties form an environment, which is unfavorable to bacterial survival or growth [41-45]. This total suppression is well exhibited by the spread plate method and highlights the huge antimicrobial potential of mullite which is high temperature calcined [46,47].

Spread plate method (SPM), Powder-Mullite at 1100 ºC				
No.	**Bacteria Type**	**Weight (g)**	**No. of colonies**	**Image**
1	*E. coli*	0.3	0	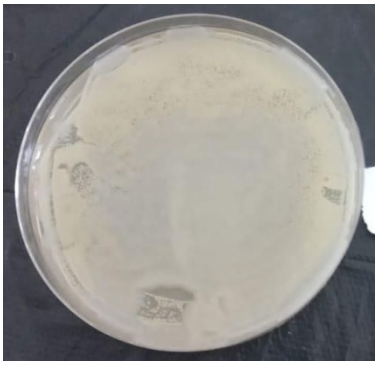
2	*S. aureus*	0.3	0	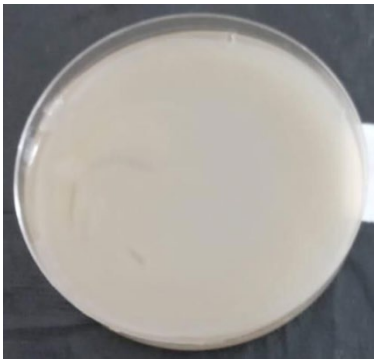

Figure 6 Spread plate method (SPM) of testing powdered mullite at temperatures of 950 ºC and against *E. coli* and *S. aureus*

4. CONCLUSIONS

Mullite prepared at 950 °C exhibited a well-defined nanostructure, as confirmed by AFM, FESEM, and TEM analyses. TEM established that the primary crystallite size averaged ~30 nm with a narrow distribution, while AFM and FESEM highlighted larger surface grains and agglomerates in the 80–120 nm range, reflecting thermal coarsening and hierarchical surface evolution. The integration of these techniques provides a comprehensive picture of mullite's microstructural development at intermediate calcination temperatures. Antibacterial assays using ADM and SPM confirmed the strong inhibitory effect of mullite pellets against both *E. coli* and *S. aureus*, with no detectable bacterial colonies observed in SPM tests. The combination of controlled nanoscale features, surface roughness, and antibacterial activity positions mullite as a promising candidate for multifunctional applications in protective coatings, environmental remediation, and biomedical devices.

References

[1] I. Alshalal, H. M. I. Al-Zuhairi, A. A. Abtan, M. Rasheed, M. K. Asmail. J. Mech. Behav. Mater. 32 (2023) 1 https://doi.org/10.1515/jmbm-2022-0280
[2] M. Sellam, M. Rasheed, S. Azizi, T. Saidani. Ceram. Int. 50 (2024) 20917 https://doi.org/10.1016/j.ceramint.2024.03.094
[3] O. Alabdali, S. Shihab, M. Rasheed, T. Rashid. 3rd inter. Scient. conf. alkafeel univ. (ISCKU 2021) (2022). https://doi.org/10.1063/5.0066860
[4] M. Rasheed, O. Alabdali, S. Shihab, A. Rashid, T. Rashid, J. Phys.: Conf. Ser. 1999 (2021) 012078 https://doi.org/10.1088/1742-6596/1999/1/012078

[5] N. Assoudi et al. Opt. Quant. Electron. 54 (2022) 9 https://doi.org/10.1007/s11082-022-03927-x
[6] R. Jalal, S. Shihab, M.A. Alhadi, M. Rasheed, J. Phys.: Conf. Ser. 1660 (2020) 012090 https://doi.org/10.1088/1742-6596/1660/1/012090
[7] S. Shihab, M. Rasheed, O. Alabdali, A.A. Abdulrahman, J. Phys.: Conf. Ser. 1879 (2021) 022120 https://doi.org/10.1088/1742-6596/1879/2/022120
[8] A. Keziz, M. Heraiz, M. RASHEED, A. Oueslati. Mater Chem. Phys. 325 (2024) 129757 https://doi.org/10.1016/j.matchemphys.2024.129757
[9] D. Kherifi, A. Keziz, M. Rasheed, A. Oueslati. Ceram. Int. 50 (2024) 30175 https://doi.org/10.1016/j.ceramint.2024.05.317
[10] A. Jaber, M. Ismael, T. Rashid, M. A. Sarhan, M. Rasheed, I. M. Sala. Eureka: Phys. Eng. 4 (2023) 29 https://doi.org/10.21303/2461-4262.2023.002770
[11] T. Rashid, M. M. Mokji, M. Rasheed. J. Optics 11 (2024) 99 https://doi.org/10.1007/s12596-024-02080-w
[12] H. K. Aity, E. Dhahri, M. Rasheed. Ceram. Int. 50 (2024) 54666 https://doi.org/10.1016/j.ceramint.2024.10.324
[13] M. Rasheed, S. Shihab, O. Alabdali, A. Rashid, T. Rashid, J. Phys.: Conf. Ser. 1999 (2021) 012077 https://doi.org/10.1088/1742-6596/1999/1/012077
[14] M. Rasheed, M. Nuhad Al-Darraji, S. Shihab, A. Rashid, T. Rashid. J. Phys.: Conf. Ser. 1963 (2021) 012058 https://doi.org/10.1088/1742-6596/1963/1/012058
[15] A. Keziz, M. Heraiz, F. Sahnoune, M. Rasheed, Ceram. Int. 49 (2023) 32989 https://doi.org/10.1016/j.ceramint.2023.07.275
[16] E. Kadri, K. Dhahri, R. Barillé, M. Rasheed. Phase Transi. 94 (2021) 65 https://doi.org/10.1080/01411594.2020.1832224
[17] D. Bouras, M. Rasheed, Opt. Quantum Electron. 54 (2022) 12 https://doi.org/10.1007/s11082-022-04161-1
[18] A. Zubaidi, L.M. Asaad, I. Alshalal, M. Rasheed, J. Mech. Behav. Mater. 32 (2023) 1 https://doi.org/10.1515/jmbm-2022-0302
[19] M. Rasheed et al., J. Phys.: Conf. Ser. 1999 (2021) 012080 https://doi.org/10.1088/1742-6596/1999/1/012080
[20] M. Rasheed, M.N. Al-Darraji, S. Shihab, A. Rashid, T. Rashid, J. Phys.: Conf. Ser. 1963 (2021) 012059 https://doi.org/10.1088/1742-6596/1963/1/012059
[21] M. Enneffatia, M. Rasheed, B. Louati, K. Guidara, S. Shihab, R. Barillé, J. Phys.: Conf. Ser. 1795 (2021) 012050 https://doi.org/10.1088/1742-6596/1795/1/012050
[22] M. Rasheed, O.Y. Mohammed, S. Shihab, A. Al-Adili, J. Phys.: Conf. Ser. 1795 (2021) 012043 https://doi.org/10.1088/1742-6596/1795/1/012043
[23] A.H. Ali, A.S. Jaber, M.T. Yaseen, M. Rasheed, O. Bazighifan, T.A. Nofal, Complexity 2022 (2022) 1 https://doi.org/10.1155/2022/9367638
[24] M. Rasheed, et al., J. Adv. Biotechnol. Exp. Ther. 6 (2023) 495 https://doi.org/10.5455/jabet.2023.d144
[25] M. Rasheed, I. Alshalal, A.A. Ashed, M.A. Sarhan, A.S. Jaber, Indones. J. Electr. Eng. Comput. Sci. 33 (2024) 653 https://doi.org/10.11591/ijeecs.v33.i1.pp653-660
[26] I.M. Mohammed, M. Rasheed, AIP Conf. Proc. 3321 (2025) 020026 https://doi.org/10.1063/5.0289719
[27] F. Boudou, A. Belakredar, A. Berkane, M. Rasheed. Not. Sci. Biol. 17 (2025) 12183 https://doi.org/10.55779/nsb17212183
[28] F. Boudou, et al., Not. Sci. Biol. 17 (2025) 12593 https://doi.org/10.55779/nsb17312593
[29] F. Boudou, A. Guendouzi, A. Belkredar. M. Rasheed, Not. Sci. Biol. 16 (2024) 13837 https://doi.org/10.55779/nsb16211837
[30] R.S. Mahmood et al. J. Mech. Behav. Mater. 34 (2025) 1 https://doi.org/10.1515/jmbm-2025-0040

[31] T. Rashid, M.M. Mokji, M. Rasheed, J. Mech. Behav. Mater. 34 (2025) 77 https://doi.org/10.1515/jmbm-2025-0074
[32] M. Rasheed, M. N. Mohammedali, F. A. Sadiq, M. A. Sarhan, T. Saidani. J. Optics (New Delhi. Print) (2024) https://doi.org/10.1007/s12596-024-01928-5
[33] A.J. Hussein, M.N. Al-Darraji, M. Rasheed, M.A. Sarhan, IOP Conf. Ser.: Earth Environ. Sci. 1262 (2023) 022007 https://doi.org/ 10.1088/1755-1315/1262/2/022007
[34] A.J. Hussein, M.N. Al-Darraji, M. Rasheed, M.A. Sarhan, IOP Conf. Ser.: Earth Environ. Sci. 1262 (2023) 022005 https://doi.org/10.1088/1755-1315/1262/2/022005
[35] T. Saidani, M. Rasheed, I. Alshalal, A.A. Rashed, M.A. Sarhan, R. Barillé, Res. Eng. Struct. Mater. 10 (2024) 743 http://dx.doi.org/10.17515/resm2023.21ma0922rs
[36] M. A. Sarhan, S. Shihab, B. E. Kashem, M. Rasheed, J. Phy.: Conf. Ser., 1879 (2021) 022122 https://doi.org/10.1088/1742-6596/1879/2/022122
[37] M. Rasheed, O. Alabdali, S. Shihab, J. Phy.: Conf. Ser. 1879 (2021) 032120 https://doi.org/10.1088/1742-6596/1879/3/032120
[38] M. Rasheed, R. Barillé, J. Non-Cryst. Solids., 476 (2017) 1 https://doi.org/10.1016/j.jnoncrysol.2017.04.027
[39] M. Rasheed, R. Barillé, Opt. Quantum Electron. 49 (2017) 99 https://doi.org/10.1007/s11082-017-1030-7
[40] F. Dkhilalli, S. M. Borchani, M. Rasheed, R. Barille, K. Guidara, M. Megdiche, J. Mater. Sci. Mater. Electron, 29(8) (2018) 6297 https://doi.org/10.1007/s10854-018-8609-z
[41] A. Boumezoued, K. Guergouri, Régis Barillé, Rechem Djamil, Mourad Zaabat, M. Rasheed, J. Alloys Compd. 791 (2019) 550 https://doi.org/10.1016/j.jallcom.2019.03.251
[42] N. Ben Azaza et al., Opt. Mater., 96 (2019) 109328 https://doi.org/10.1016/j.optmat.2019.109328
[43] M. M. Abbas, M. Rasheed, J. Phys. Conf. Ser. 1795 (2021) 012059 https://doi.org/10.1088/1742-6596/1795/1/012059
[44] M. Rasheed, SuhaShihab, O. Alabdali, H. H. Hassan, J. Phys. Conf. Ser., 1879(3) (2021) 032113 https://doi.org/10.1088/1742-6596/1879/3/032113
[45] Rida Ahmed Ammar. Experimental and Theoretical NANOTECHNOLOGY 2 (2018) 1 https://doi.org/10.56053/2.1.1
[46] M. Mourad Mabrook, Experimental and Theoretical NANOTECHNOLOGY 2 (2018) 103 https://doi.org/10.56053/2.2.103
[47] F. M. Shamsudin, S. Radiman, Y. Abdullah, N. A. Hamid, Experimental and Theoretical NANOTECHNOLOGY 3 (2019) 27 https://doi.org/10.56053/3.1.27